ACS APPLIED MATERIALS & INTERFACES

www.acsami.org

Research Article

Novel Binder with Cross-Linking Reconfiguration Functionality for Silicon Anodes of Lithium-Ion Batteries

Ruilai Ye, Jiaxiang Liu, Jianling Tian, Yi Deng, Xueying Yang, Qichen Chen, Peng Zhang,* and Jinbao Zhao*

Cite This: *ACS Appl. Mater. Interfaces* 2024, 16, 16820−16829

Read Online

ACCESS | Metrics & More | Article Recommendations | Supporting Information

ABSTRACT: Silicon is expected to be used as a high theoretical capacity anode material in lithium-ion batteries with high energy densities. However, the huge volume change incurred when silicon de-embeds lithium ions, leading to destruction of the electrode structure and a rapid reduction in battery capacity. Although binders play a key role in maintaining the stability of the electrode structure, commonly used binders cannot withstand the large volume expansion of the silicon. To alleviate this problem, we propose a PGC cross-linking reconfiguration binder based on poly(acrylic acid) (PAA), gelatin (GN), and *β*-cyclodextrin (*β*-CD). Within PGC, PAA supports the main chain and provides a large number of carboxyl groups (−COOH), GN provides rich carboxyl and amide groups that can form a cross-linking network with PAA, and *β*-CD offers rich hydroxyl groups and a cone-shaped hollow ring structure that can alleviate stress accumulation in the polymer chain by forming a new dynamic cross-linking coordination conformation during stretching. In the half cell, the silicon negative prepared by the PGC binder exhibited a high specific capacity and capacity maintenance ratio, and the specific capacity of the silicon negative electrode prepared by the PGC binder is still 1809 mAh g^{-1} and the capacity maintenance ratio is 73.76% following 200 cycles at 2 A g^{-1} current density, indicating that PGC sufficiently maintains the silicon negative structure during the battery cycle. The PGC binder has a simple preparation method and good capacity retention ability, making it a potential reference for the further development of silicon negative electrodes.

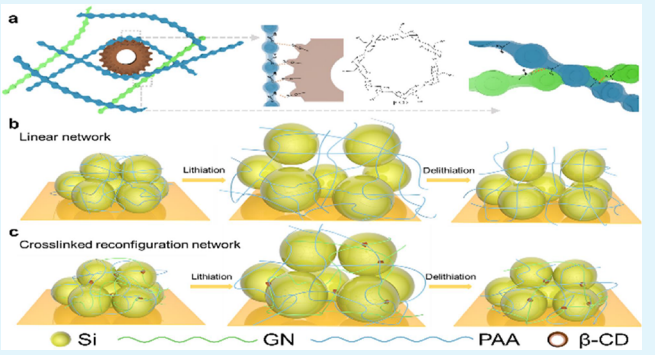

KEYWORDS: *silicon anode, β-cyclodextrin, cross-linking reconfiguration binder, high performance*

1. INTRODUCTION

The development of electric vehicles limited by the capacity of graphite anode (372 mAh g^{-1}, LiC_6) has led to the emergence of range anxiety, necessitating the exploration of high-energy negative electrode materials.[1] Silicon is recognized as a conceivable anode material for high-energy-density lithium-ion batteries owing to its high theoretical capacity (4200 mAh g^{-1}, $Li_{4.4}Si$), low working potential, and abundant reserves.[2,3] Nevertheless, unlike the insertion/extraction mechanism of lithium-ion storage in graphite, silicon anodes undergo alloying/dealloying transformations during electrochemical reactions, leading to significantly higher volume expansion and shrinkage (>300%) upon cycling than the insertion/extraction process. This causes fragmentation of silicon electrodes, instability of the solid electrolyte interface (SEI), loss of electrical contact within the electrode film, and ultimately, a rapid deterioration of capacity, hindering the large-scale applicability of silicon anodes.[4,5]

To resolve the aforementioned issues, the stable structure of the silicon anode can be maintained from both the material and electrode aspects by designing nanostructures,[6] modifying the carbon coating,[7] or introducing an artificial SEI layer and high-performance binders.[8,9] To address the significant volume expansion incurred by the alloying process, the stable electrode structure is the key factor to exert the performance of the material after having excellent electrode materials, which are modified from the material scale.[10−12] High-performance binders have been demonstrated to maintain the structure of the electrode while exerting the material capacity. Besides high performance, these binders have relatively low production costs and do not change existing cell preparation processes, thus receiving widespread research attention.[13]

The binder plays a crucial role in maintaining the integrity of the electrode structure by relieving volume changes and maintaining electrical contact with silicon particles, which

Received: January 11, 2024
Revised: March 14, 2024
Accepted: March 14, 2024
Published: March 25, 2024

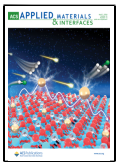

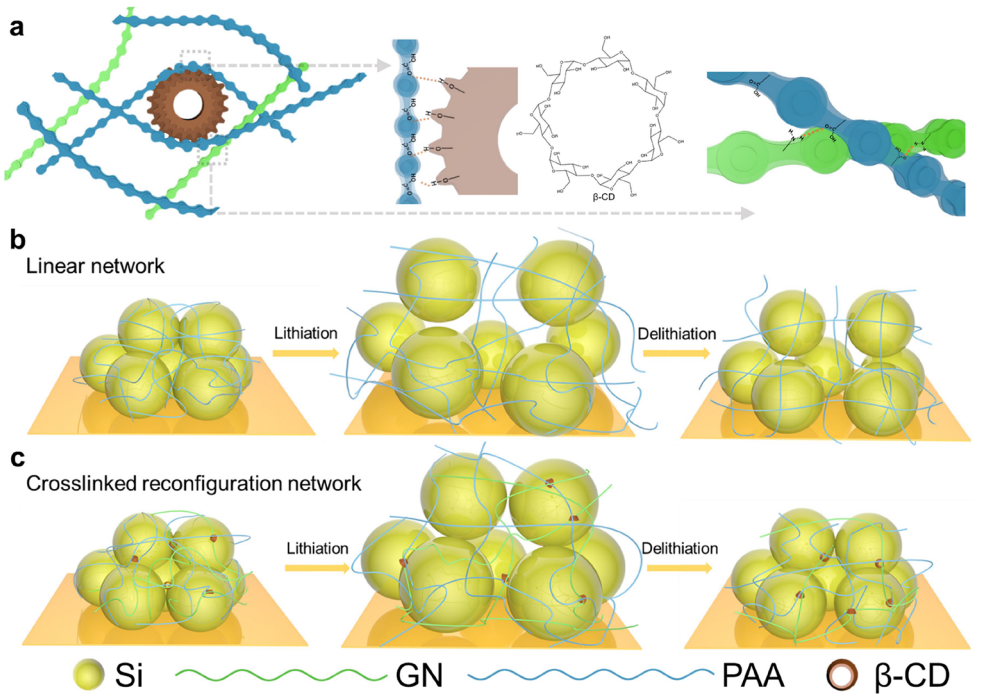

Figure 1. (a) Schematic diagram of the internal mechanism of PGC and structure of β-CD. Action mechanisms of (b) PAA and (c) PGC binders in the battery cycle.

connect the active substance to the conductive agent and current collector.[14] However, commercial binders for instance polyvinylidene difluoride (PVDF) and carboxymethyl cellulose (CMC) have difficulty adapting to the volume expansion of silicon owing to their linear molecular structures, fragility, and poor interaction force.[15,16] Recently, many studies have employed high-performance binders—such as self-healing, covalent bond cross-linking, branching architecture, and hydrogen bond cross-linking binders—to meet the requirements of high elasticity, self-healing, and interface compatibility in silicon anodes.[17−20] Furthermore, the introduction of abundant functional groups—including carboxyl (−COOH), hydroxyl (−OH), and amine ($-NH_2$)—have been demonstrated to effectively stabilize the silicon structure and electrode plate architecture.[21] The mechanism can be concluded that surface binding could be formed between polar groups and hydroxyl functional (−OH) groups on the surface of silicon particles. In addition, hydrogen bonds formed with abundant polar groups on polymer chain segments may form a dynamic cross-linking network in response to the huge volume change of silicon particles, preventing the continuous generation of the SEI.[22] For example, Wang and co-workers obtained an interpenetrated gel polymer binder by cross-linking poly(vinyl alcohol) (PVA) and poly(acrylic acid) (PAA), forming a strong binding network through interactions between the carboxyl and hydroxyl groups.[23] Tang and Zhang and co-workers employed thiourea to develop a self-healing polymer binder and cushion the massive volume expansion during the lithiation/delithiation process.[24] However, multiple volume expansions lead to uneven stress consumption and inhibit the hydrogen bond effect, resulting in an active material loss of the electrical contact and the collapse of the electrode structure.

We propose a high-performance binder that achieves stress dissipation by cross-linking reconfigurations of a slightly conical hollow-cylinder ring-structure polymer, obtained by combining PAA, gelatin (GN), and β-cyclodextrin (β-CD) denoted as PGC. The carboxyl group in the PAA and the polar group in the GN form a stable and flexible cross-linking network owing to hydrogen bonding between the GN, PAA, and silicon particles. The β-CD is composed of seven glucose molecular units and characterized by a three-dimensional cone-shaped hollow cylindrical structure, which has some amount of hydroxyl groups.[25] This combination exhibits excellent mechanical properties through hydrogen bonding interactions and the movement of cyclic molecules, maintaining the stability of the silicon negative structure and enabling stable cycling. First, the −OH on the outer surface of β-CD can form hydrogen bonds with polar groups in the polymer network. Furthermore, owing to the peculiar cylindrical ring structure of β-CD, the pattern of cross-linking transforms from point cross-linking along the linear polymer to planar cross-linking, providing a flexible combination. In addition, the unique structure of β-CD can buffer the stress caused by deformation through molecular motion, such as rotation and slip, as the polymer network stretches, form a new dynamic cross-linking coordination conformation in the polymer network, and coordinate with the sliding motion of the PAA and GN molecular chains to constantly adapt to deformation, thereby maintaining the structure of the negative electrode.

Thus, the addition of β-CD to the PG network to form a cross-linking reconfiguration polymer network greatly improves the mechanical properties of the binder, such as its excellent tensile rate. Furthermore, the addition of GN, which contains many polar groups and hydrophilic/hydrophobic amphoteric segments, enhances the binder's adhesion. Owing to its excellent mechanical properties, the PGC binder helps stabilize the electrode configuration in the course of charge and discharge processes, maintain electrical contact, reduce the increase in SEI, and achieve stable cycle performance. According to test results, the PGC binder exhibits an excellent capacity retention ability in silicon/lithium half cells, with the

https://doi.org/10.1021/acsami.4c00590
ACS Appl. Mater. Interfaces 2024, 16, 16820−16829

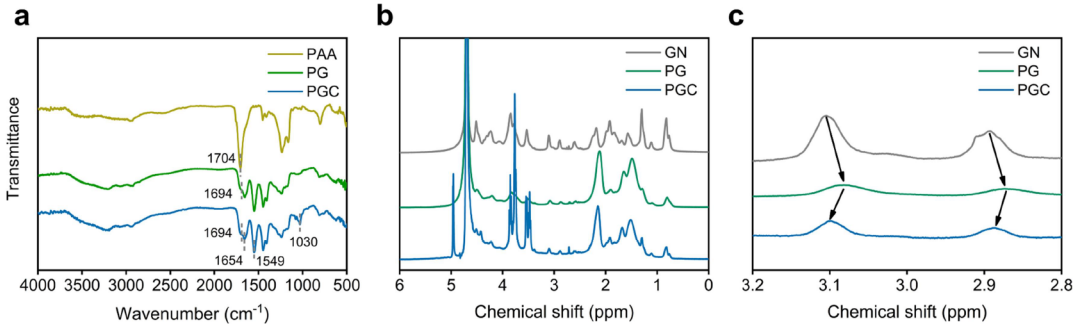

Figure 2. (a) FTIR spectra of PAA, PG, and PGC polymers. (b) ^{1}H NMR spectra of different polymers. (c) Enlarged view of the ^{1}H NMR spectrum.

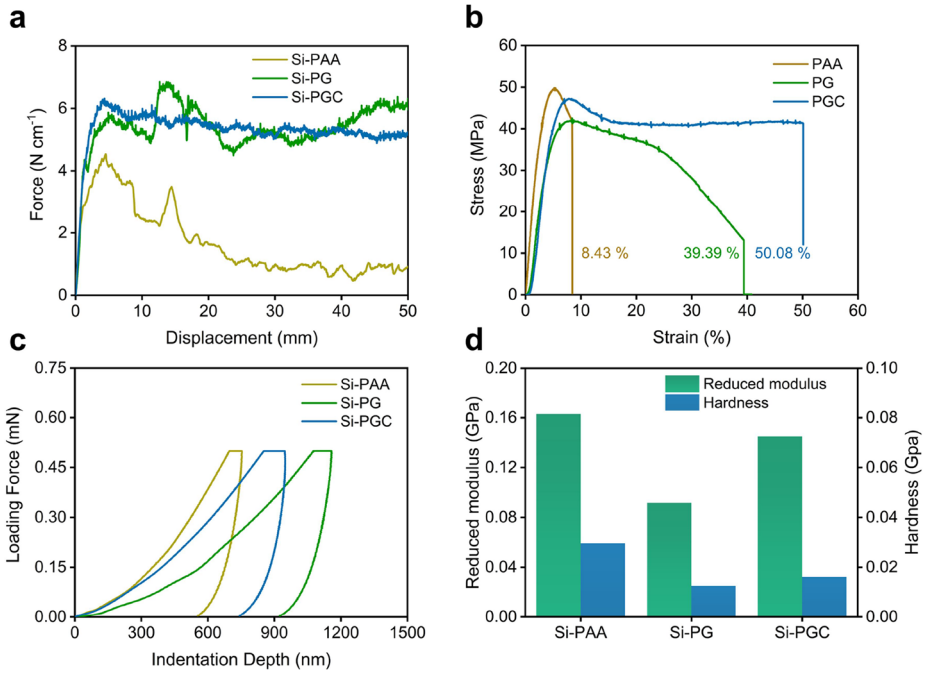

Figure 3. (a) Strain−stress curves of PAA, PG, and PGC films. (b) Peeling curves and (c) load−indentation depth curves of electrodes with different binders. (d) Reduced moduli and hardness of different electrodes.

resulting silicon anode achieving a specific capacity of 1809.0 mAh g^{-1} following 200 cycles at a heavy current density of 2.0 A g^{-1}. This is a significant improvement over Si-PAA (639.1 mAh g^{-1}) as well as Si-PGN (1229.1 mAh g^{-1}) with a silicon loading of 0.7−0.85 mg cm^{-2}. The PGC binder exhibited a tensile ratio of 50.08% in the tensile test, reflecting its strong stress dissipation ability. In contrast to conventional point-and-line cross-linking, for enhancing the performance of silicon anodes we employed an alternate energy dissipation strategy by cross-linking reconfiguration of a conical cylindrical ring-structure polymer, which provides a reference for the study of silicon negative electrodes.

2. RESULTS AND DISCUSSION

The direct mixing of PAA and GN at room temperature resulted in rapid precipitation, and the lack of fluidity indicated that a cross-linked network was formed through an acid−base reaction. Therefore, ammonia−water was first added to PAA solution to counteract the carboxyl groups and inhibit the cross-linking reaction (Figure S2). Subsequently, the solution was mixed with GN. The amino group neutralized by the carboxyl group evaporated during the drying process, and the polymer was recross-linking in the electrode.[26−28]

Owing to its annular structure, the addition of β-CD to the cross-linking network may result in chain slippage between polymer chains through the sliding and rotation of β-CD, dissipating the stress and forming a new cross-linking coordination conformation in the polymer network as a consequence of deformation. Through the coordination of β-CD with the cross-linking network formed by PAA and GN, the polymer network can withstand considerable deformation and maintain sufficient strength to adapt to the drastic expansion of silicon. Figure 1a illustrates the internal bond mechanism of the PGC cross-linking reconfiguration, with Figure 1b depicting the failure mechanism of the PAA adhesive. Owing to its strong rigidity, the PAA network is vulnerable to fractures during the cycling process, resulting in a reduced adhesion effect. However, PGC can effectively alleviate stress through the cross-linking reconfiguration of β-CD, thereby maintaining good adhesion performance, as shown in Figure 1c.

The internal structures of the cross-linking reconfiguration networks were examined using FTIR, as shown in Figure 2a.

https://doi.org/10.1021/acsami.4c00590
ACS Appl. Mater. Interfaces 2024, 16, 16820−16829

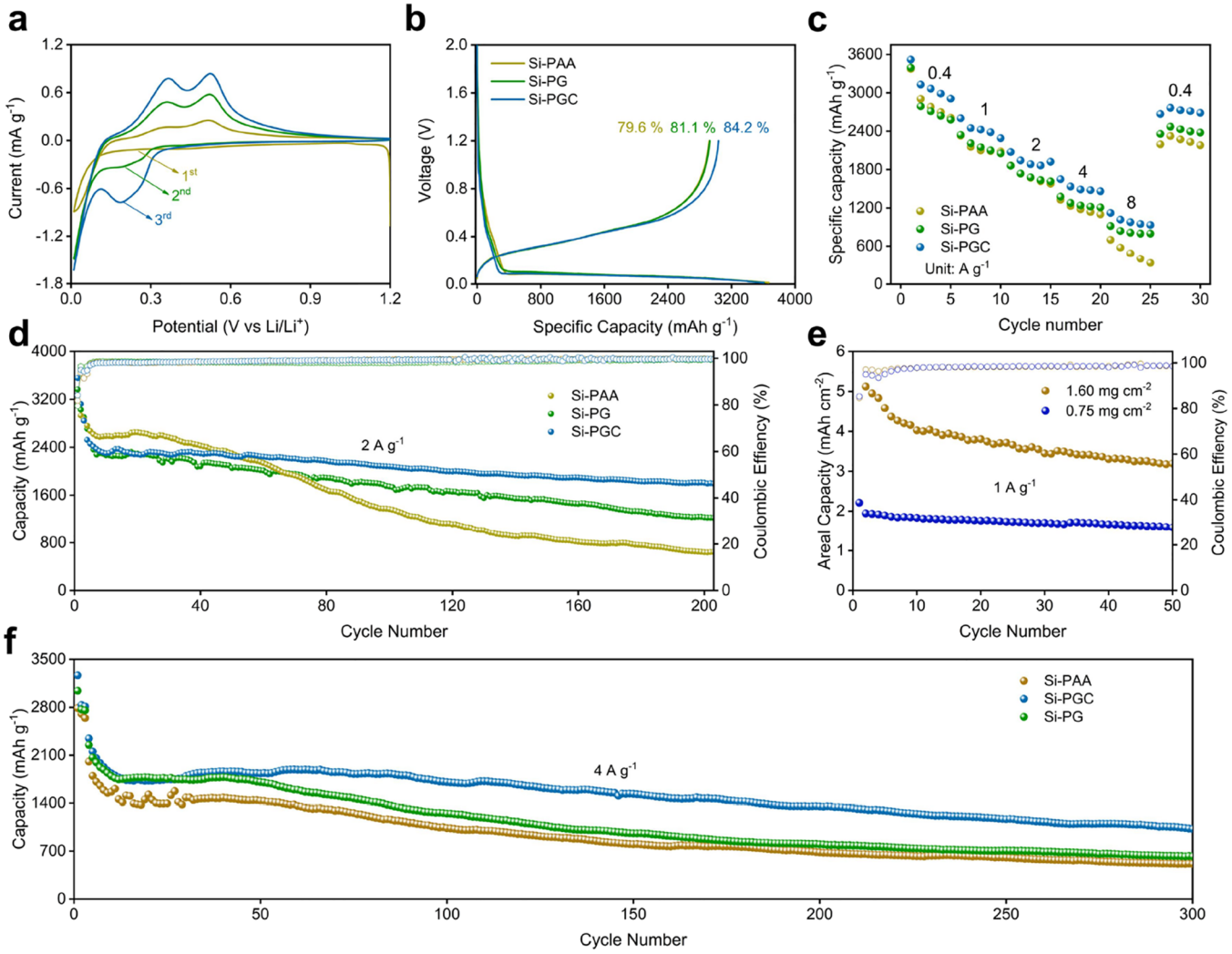

Figure 4. (a) CV curves of the Si-PGC electrode at 0.1 mV s^{-1}. (b) Initial discharge−charge profiles of different electrodes at 0.4 A g^{-1}. (c) Rate performance of the electrodes with different binders. (d) Cycling performance of the electrodes at 2 A g^{-1}. (e) Cycling performance for Si-PGC with different Si loadings at 1 A g^{-1}. (f) Long cycling performance of electrodes at 4 A g^{-1}.

Following the introduction of GN, the characteristic peak of carboxyl group (−COOH) PAA at 1704 cm^{-1} shifted to 1694 cm^{-1}, indicating that the addition of GN leads to cross-linking.[29,30] Simultaneously, the −C═O and −N−H bonds of the amide group in gelatin correspond to two new characteristic peaks at 1654 and 1549 cm^{-1}.[31] In the infrared spectrum of the PGC polymer, the appearance of a new characteristic peak at 1030 cm^{-1} is due to the −C−O−C− structure in β-CD.[32] Meanwhile, the infrared spectrum of PAA mixed with β-CD shows that the peak of carboxyl group (−COOH) PAA decreases from 1704 to 1696 cm^{-1}, indicating that abundant hydroxyl groups on the surface of β-CD form hydrogen bonds with the abundant −COOH in PAA. To further elucidate cross-linking in the PGC adhesive network, we deployed nuclear magnetic resonance (NMR) spectroscopy. The NMR spectrum in Figure 2b shows that upon mixing PAA with GN, the hydrogen atoms of GN shift toward a higher field, indicating an interaction between PAA and GN. Interestingly, following the addition of β-CD, the hydrogen atoms shift toward a lower field, indicating that β-CD weakens interactions within the system. This is ascribed to the cyclic structure and relatively large molecular weight of β-CD, which forms cavities within the cross-linking network, thereby reducing interactions between PAA and GN. This weakening effect favors the molecular motion of β-CD in the polymer network. Moreover, in the NMR spectrum of the PAA/β-CD system, the hydrogen atoms of β-CD also shift toward a higher field upon the addition of PAA, indicating the formation of hydrogen bond cross-linking between β-CD and PAA as the interaction between PAA and GN weakens (Figure S3). Through infrared and NMR characterizations, it is evident that β-CD plays a role in cross-linking and sliding within the polymer network. Owing to the rich polar groups and cross-linking, cohesion within the polymer network can be greatly enhanced while maintaining structural stability and adapting to the volume expansion of the silicon negative electrode.[33]

Mechanical characterization of the binder film was performed via stress−strain analysis. As shown in Figure 3a, the PGC film achieved 50.08% strain before fracture, which was much higher than that of PAA (8.43%) and PG (39.39%), indicating that the PGC binder network with cross-linking reconfiguration is strong, adaptable to deformation, and able to withstand high stress. The β-CD component in the cross-linking reconfiguration binder dissipates stress in the polymer network and adapts to deformation through molecular ring movement, thereby reconfiguring the cross-linking coordina-

https://doi.org/10.1021/acsami.4c00590
ACS Appl. Mater. Interfaces 2024, 16, 16820−16829

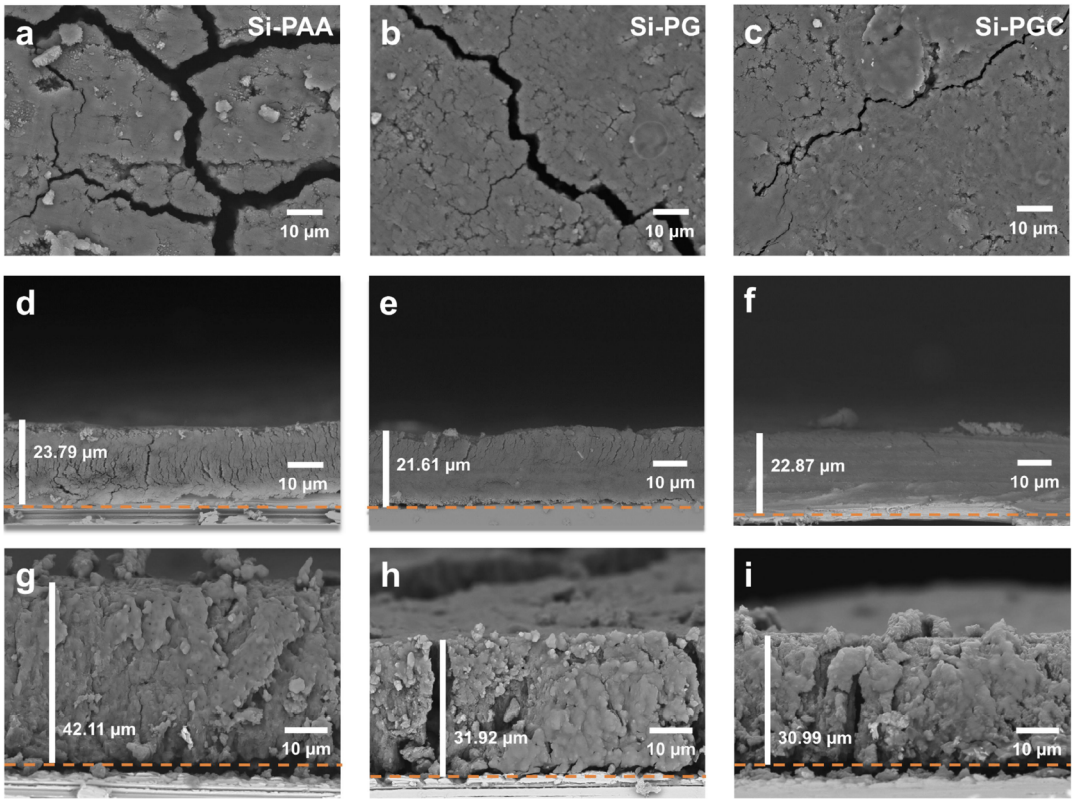

Figure 5. (a−c) SEM image of a silicon electrode surface following 100 cycles at 2 A g^{-1}. (d−f) Cross-sectional scan images of silicon electrodes initially and (g−i) following 100 cycles.

tion. Consequently, the PGC polymer has excellent elongation properties. The cross-linking action and rigid structure of β-CD ensure sufficient network rigidity. Thus, the PGC binder exhibits excellent elongation and strength simultaneously.

Peeling tests were conducted at a strain rate of 10 mm min^{-1}. As exhibited in Figure 3b, the peel strengths of Si-PG and Si-PGC anode are higher than that of Si-PAA. The average adhesion of Si-PGC is 5.2 N, which is close to that of Si-PG (5.5 N) and much higher than that of Si-PAA (1.6 N). The increase in adhesion is attributed to the cross-linking effect of GN, which enhances the interaction between the polymers while increasing the cohesion of electrodes. In addition to the interactions between polymers, abundant polar groups interacted with the oxide on the surface of the copper foil, strengthening the adhesion of the active material to the foil. After peeling, the Si-PAA electrode exposed more copper foil, whereas the Si-PG and Si-PGC electrodes did not expose the copper foil, as shown in Figure S4, which intuitively indicates improved electrode adhesion following the addition of GN.

Typical load−displacement curves of various binder electrodes are exhibited in Figure 3c. The indentation depth of the Si-PGC electrode is lower than that of the Si-PG electrode and higher than that of the Si-PAA electrode for a load of 0.5 mN. The decreasing moduli and hardness of different electrodes acquired by calculating load−displacement curves are shown in Figure 3d. These results correlate with the performance results indicated by the strain−stress curves of the binder: in the silicon electrode, a moderate modulus and hardness endow the electrode with better stress resistance and adaptability to volume expansion. From the perspective of mechanical properties, the PGC binder is therefore helpful in achieving stable electrode cycling.

The wettability of the electrode and electrolyte influences the kinetics of the electrode. We analyzed the wettability with different binders using a contact angle test, demonstrating that the Si-PGC electrode has a lower contact angle (16°) than Si-PAA (25°) and Si-PG (18°) electrodes (Figure S5). This indicates that the superior wettability of the PGC binder is conducive to Li^+ diffusion within the silicon electrodes.

We conducted additional experiments to examine the electrochemical stability of the PGC binder. The CV curves are set to a voltage range of 0.01−3.0 V versus that based on coin-type cells. Figure S6 shows that the CV curve of the polymer film is identical to that of pure copper foil, and there is no redox peak for polymer decomposition, indicating that the PGC binder has good stability under the working potential.

Silicon anodes prepared with various binders were assembled into half cells for evaluation. First, cyclic voltammetry (CV) tests in the voltage range 0.01−1.2 V at 0.1 mV s^{-1} were performed on the silicon anode prepared by using each binder. As shown in Figure 4a, the cathodic peak at ≈0.55 V during the first cathode scan corresponds to the formation of SEI, whereas the peak at 0.1 V is caused by the reaction of Li^+ with silicon to transform into a lithium−silicon alloy. The delithium process at the anode showed oxidation peaks at 0.37 and 0.52 V.[34] In subsequent cycles, the peak at 0.19 V is associated with the transition from a silicon to lithium silicon alloy. Si-PAA and Si-PG exhibit similar curves (Figure S7), reflecting the normal redox mechanism of silicon anode.

Figure 4b reveals the initial charge−discharge profiles. Si-PGC shows an incipient discharge capacity of 3606 mAh g^{-1} at 0.4 A g^{-1}, with the initial Coulombic efficiency of 84.2% exceeding Si-PAA (79.6%) and Si-PG (81.1%). A rate test of the silicon negative electrode was performed at different

https://doi.org/10.1021/acsami.4c00590
ACS Appl. Mater. Interfaces 2024, 16, 16820−16829

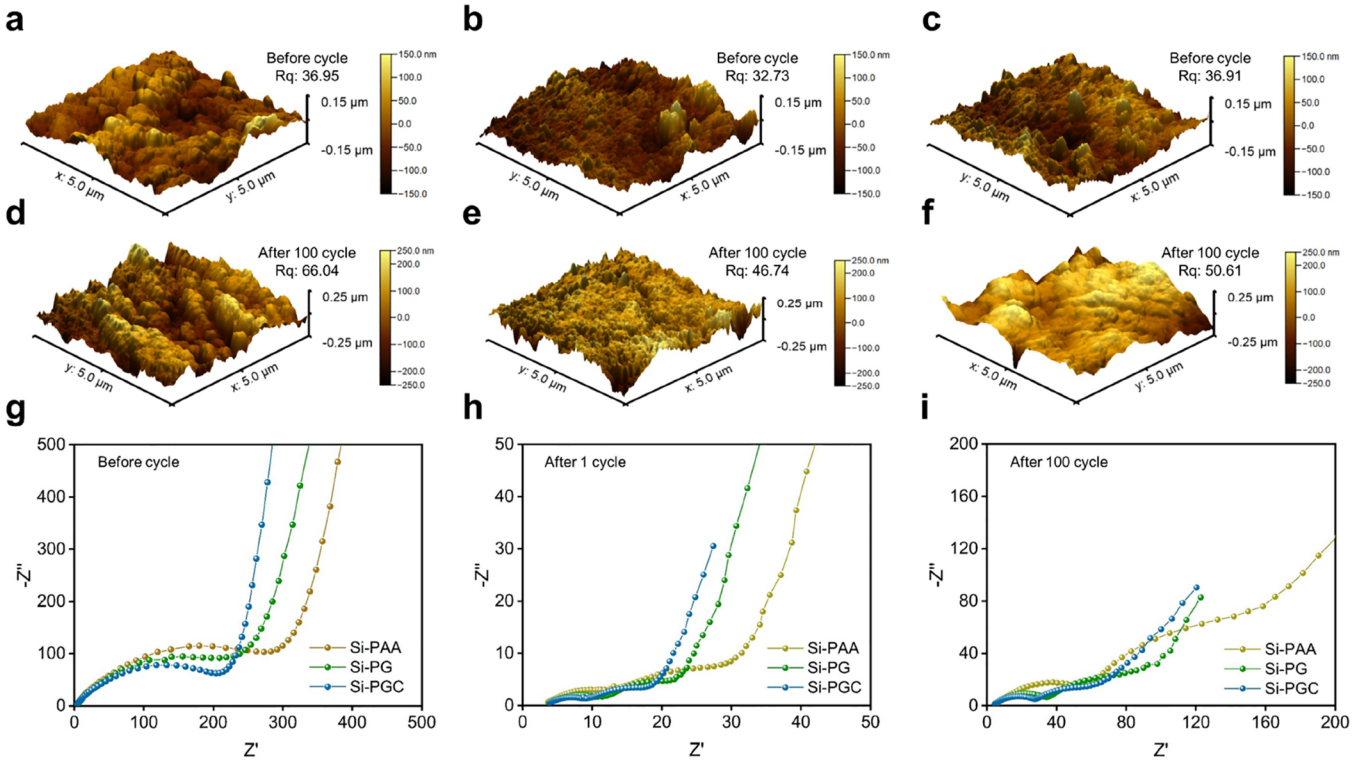

Figure 6. AFM images of (a) Si-PAA, (b) Si-PG, and (c) Si-PGC anodes before cycling. AFM images of (d) Si-PAA, (e) Si-PG, and (f) Si-PGC following 100 cycles at 2 A g^{-1}. EIS results of Si-PAA, Si-PG, and Si-PGC anodes (g) before cycling, (h) following 1 cycles, and (i) following 100 cycles.

current densities. Owing to the PGC binder, the Si-PGC can tightly connect the silicon particles to the conductive agent while maintaining electrical contact. Subsequently, the electrode retains a capacity of 931.6 mAh g^{-1} even at 8 A g^{-1} (Figure 4c), which is higher than those of Si-PAA (333.5 mAh g^{-1}) and Si-PG (798.2 mAh g^{-1}). When the current is recovered to 0.4 A g^{-1}, the capacity returns to 2765.4 mAh g^{-1}, manifesting that PGC plays a key role in maintaining structural stability. Figure 4d shows that Si-PGC still maintains a capacity of 1809.0 mAh g^{-1} at 2 A g^{-1} while demonstrating a capacity retention of 73.5% following 200 cycles, which is significantly better than Si-PAA (639.1 mAh g^{-1}, 24.8%) and Si-PG (1229.1 mAh g^{-1}, 51.4%). The above battery performance test results illustrate that the PGC binder is better than simple line cross-linking in long cycles while maintaining high capacity in electrode cycles.

Figure 4f illustrates the long-term cycling performance of anodes with various binders at 4 A g^{-1}. Following 300 cycles, the capacity remains at 1023.8 mAh g^{-1}. When the high-load silicon electrode was examined, the Si-PGC with a load of 1.6 mg cm^{-1} displayed an areal capacity of 3.19 mAh cm^2 at 1 A g^{-1} following 50 cycles (Figure 4e). Illustrating that the electrochemical performance of PGC binders with a cross-linking reconfiguration function in a silicon negative electrode is better than that of ordinary linear cross-linking-modified binders. Carboxyl group-rich PAA, which occupies the largest proportion, not only cross-links with functional groups such as −NH and −OH, but also forms hydrogen bonds with hydroxyl groups on the surfaces of silicon particles, which increases the interaction inside the electrode sheet while enhancing the adhesion ability.[35,36] Because GN has many carboxyl and amino groups, it easily cross-links with other polymers. The polymer film was found to exhibit better elasticity after addition of GN to the PAA matrix. As a cyclic polymer with a unique structure and rich hydroxyl groups on its surface, β-CD can be cross-linking with polar groups in the network and exhibit a molecular movement effect. When the polymer network deforms, the stress concentrated through the molecular ring motion of β-CD is dispersed and a new cross-linking coordination conformation is established and transformed to adapt to the deformation. Thus, the generated strain can be dissipated in the intense volume expansion by adding β-CD, to improve the stabilization of capacity during cycling of silicon negative electrodes.

To further verify the ability of the PGC binder to maintain the electrode structure, we employed SEM for observation. Before cycling, all electrode surfaces were smooth and flat, as shown in Figure S9. However, following 100 cycles at 2 A g^{-1}, multiple wide cracks on the surface of the Si-PAA electrode emerge, whereas the Si-PG electrode emerges significantly less and smaller cracks. The Si-PGC electrode showed the fewest cracks with the narrowest width (Figure 5a−c). SEM images of the surface demonstrated that the higher modulus of the PGC binder can withstand the stress caused by volume expansion and that the binder can dissipate the stress caused by strain through the molecular motion action, thereby maintaining a good electrode structure. The digital image of the electrode after 100 cycles shown in Figure S10 is consistent with the above results. Figure 5d−f presents cross-sectional SEM images. The thicknesses of the pristine Si-PAA, Si-PG, and Si-PGC electrodes were 23.79, 21.61, and 22.87 μm, respectively. Figure 5g−i presents that the thickness of Si-PGC increased to 30.99 μm following 100 cycles. The 35% expansion rate of Si-PGC was drastically lower than that of Si-

https://doi.org/10.1021/acsami.4c00590
ACS Appl. Mater. Interfaces 2024, 16, 16820−16829

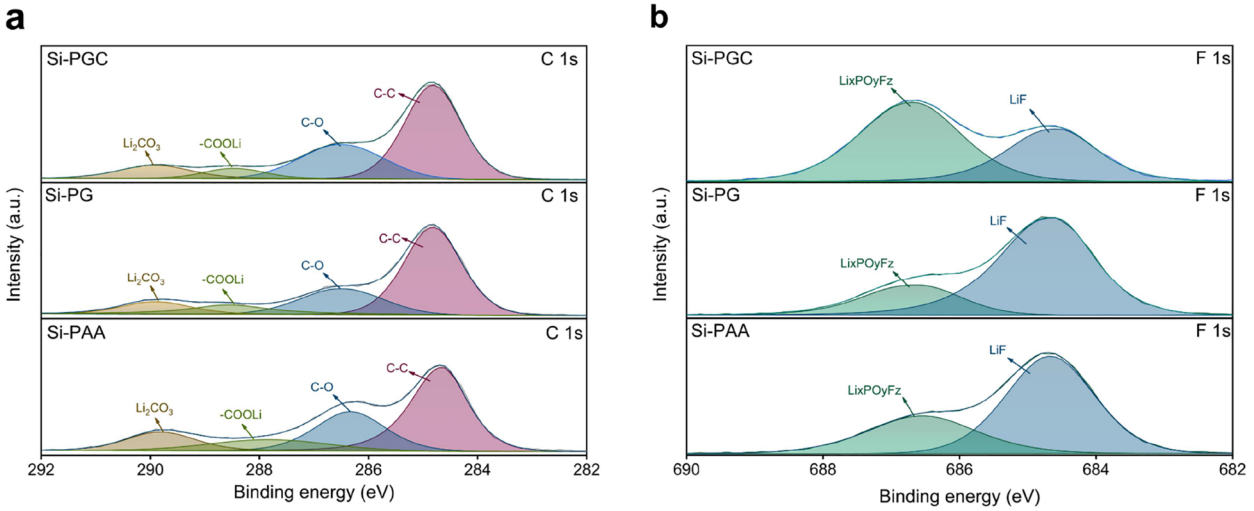

Figure 7. XPS (a) C 1s and (b) F 1s spectra of Si-PGC, Si-PG, and Si-PAA electrodes following 100 cycles at 2 A g^{-1}.

PAA (77%) and Si-PG (47%), further illustrating the inhibition effect of negative electrode volume expansion in the PGC binder.

Atomic force microscopy (AFM) was used to measure variability in the anode surface roughness to observe the microscopic surface structure of the anode. Based on 3D topography of the electrode surface (Figure 6a−c), the three electrodes exhibited similar surface roughness before cycling, which match the SEM image. The 3D surface roughness of Si-PGC slightly increased to 50.61 nm (Figure 6f) following 100 cycles at 2 A g^{-1}. In comparison, Si-PAA exhibited a sharp increase in surface roughness (66.04 nm). Although Si-PG exhibited a slightly lower surface roughness, the 3D surface image of Si-PGC showed a smoother surface. The smaller change in surface roughness and smoother 3D surface image confirm the role of the cross-linking reconfiguration network based on PGC binders in suppressing volume expansion and maintaining the electrode structure.

The electrode structure characterization results show a strong correlation with the cycle data of the battery, proving that the PGC binder slows capacity attenuation by stabilizing the electrode structure.

The electrochemical kinetics of Si anodes before and after cycling were evaluated using EIS. As shown in Figure 6g−i, the fitting results of the EIS spectra of the silicon electrode are two semicircles and a straight line. Solid electrolyte interfacial resistance (R_{SEI}) is represented by a semicircle in the high-frequency range, whereas the charge transfer resistance (R_{ct}) is in the midfrequency range. The fitting confirms that the Si-PGC electrode has the lowest resistance among the three electrodes. As previously mentioned, the PGC binder is more closely related to the electrolyte, which reduces the internal impedance of the battery. As shown in Table S1, R_{ct} (25.78 Ω) and R_{SEI} (25.63 Ω) of the Si-PGC electrode were also minimal after at 2 A g^{-1} following 100 cycles. The lower resistance is dependent on the cross-linking reconfiguration of the polymer network that adapts to the volume expansion of silicon, leading to fewer cracks on the electrode surface after cycling. Because the electrode structure is maintained, a stable SEI layer is generated, and favorable electrical contact is ensured.

The stability of the silicon anode and ion transport were significantly influenced by the SEI layer. To analyze the chemical composition of the SEI layer, XPS was used to characterize the silicon electrode following 100 cycles. Figure 7a hints that the peaks in the XPS C 1s spectra are located at 284.8 eV (C−C), 286.5 eV (C−O), 288.0 eV (−COOLi), and 290.0 eV (Li_2CO_3).[37] Contrast Si-PG and Si-PAA electrodes, the Li_2CO_3 and −COOLi peaks of the Si-PGC anode are weakest, indicating that less Li_2CO_3 and −COOLi are generated on the Si-PGC surface. This result reflects the PGC binder maintaining a stable electrode structure and reducing rupture of SEI, leading to the minimal amount of electrolyte to be decomposed. Figure 7b presents F 1s spectra of two peaks at 684.7 eV (LiF) and 686.8 eV ($Li_xPO_yF_z$).[38,39] LiF is an excellent ionic conductor with high mechanical strength, and $Li_xPO_yF_z$ affects the flexibility of the SEI layer; thus, the ratio of the two compounds plays a crucial role in stabilizing the electrode structure. Figure 7b shows that the F 1s spectrum of the Si-PGC electrode surface has an appropriate ratio of $Li_xPO_yF_z$ to LiF, which ensures the Li^+ transport kinetics and flexibility of the SEI, avoiding excessive contact with the electrolyte and reducing resistance.[40] These results indicate that the cross-linking reconfiguration network can inhibit electrolyte decomposition, form a more compatible SEI, and improve ion transport, which is in line with EIS results.

To verify the advantages of the cross-linking reconfiguration network structure in maintaining the stability of the silicon negative electrode, we replaced β-CD with PVA, a one-dimensional chain polymer containing hydroxyl groups. The 1D cross-network binder prepared with PVA, PAA, and GN using the same method and ratio is referred to as PGA. First, we performed a stress−strain analysis to mechanically characterize the PGA film, as shown in Figure S12. The 29.46% elongation exhibited by PGA was less than the elongation of 50.08% of that of PGC, and the curve was similar to that of PG. However, the maximum stress was only 27.7 MPa, which is much smaller than the values of 47.2 and 41.8 MPa obtained by PGC and PG, respectively. Because PVA is a flexible chain segment, the flexibility of the polymer network system is elevated following the addition of PVA; however, this does not provide sufficient strength.[4,41] Moreover, PVA is only a one-dimensional chain, and the coordination conformation of the polymer network is locked between the polymer chains; as stress accumulates during the stretching process, the chain cannot adapt to the deformation by transforming the cross-

https://doi.org/10.1021/acsami.4c00590
ACS Appl. Mater. Interfaces 2024, 16, 16820−16829

linking coordination conformation.[42] Ultimately, the cross-linking structure is destroyed. In contrast, the ring-shaped β-CD dissipates stress through molecular ring motion, establishes a new cross-linking coordination conformation in the network, and thereby exhibits much better elongation, as its rigid structure and cross-linking action ensure a high tensile strength. Our results demonstrate that different polymer structures affect the mechanical properties of the binder network, even within the same group, further explaining the excellent tensile properties of the new cross-linking reconfiguration binder. We also mixed the PGA binder with silicon particles and a conductive agent to prepare a Si-PGA electrode. Under the same test conditions, the cyclic performance of Si-PGA was significantly lower than that of Si-PGC (Figure S12), demonstrating the advantage of the ring-slip polymer network structure in maintaining the cyclic stability of the silicon electrode.

3. CONCLUSIONS

We propose a novel adhesive with cross-linking reconfiguration functionality, wherein PAA serves as the supporting main chain that provides abundant carboxyl groups (−COOH) to form a cross-linking network with GA. β-CD, which possesses abundant hydroxyl groups and a cyclic structure, can form hydrogen bonds cross-linking with PAA while relieving stress accumulation in the polymer chains through molecular ring motion to reconfigure cross-links. In half-cell experiments, the silicon anode prepared with a PGC adhesive achieved 1809 mAh g^{-1} following 200 cycles at 2 A g^{-1}, with a capacity maintenance ratio of 73.5%. Cross-linking in the PGC system was investigated, and a comparison between linear and cyclic polymers confirmed the improved performance of the latter. In summary, we formulated a simple strategy to enhance the stability and cycling performance of silicon anodes.

4. EXPERIMENTAL SECTION

4.1. Synthesis of PGC. First, 1.0 g of PAA was dispersed in 9 mL of water with mechanical stirring for 5 h, and GN solution (10%) was prepared from 1 g of GN and 9.0 g of deionized water temperature of 50 °C. β-Cyclodextrin was dissolved in deionized water to form a 1.5% solution.

After ammonium hydroxide solution (0.18 g) was then added to neutralize PAA solution (3.6 g, 10 wt %) stirring at room temperature for 2 h, GN solution (0.9 g, 10 wt %) was added. This mixture was stirred for 6 h before adding 0.5 g of β-CD solution. The PGC binder was obtained by stirring for 4 h. PG binder is obtained without adding β-cyclodextrin.

4.2. Preparation of Electrodes. Mixing silicon powder was mixed with super P and binders (weight ratio of 60:20:20). Applying the slurry mixed evenly paste to the copper foil using a spatula then dried at 80 °C in a vacuum oven for 24 h.

4.3. Electrochemical Tests. For half cells, lithium metal as counter electrode and obtained electrodes were used as working electrodes, and Celgard 2500 membrane as a separator. Assembling CR 2032-type coin cells were placed in an Ar-filled glovebox. The electrolyte contained 1.0 M LiPF6 in EC/DEC (v/v 1:1) with 10 wt % fluoroethylene carbonate (FEC) additive. The half cells galvanostatic charge/discharge test were cycled between 0.01 and 1.2 V, using the Neware battery test. The Si anodes were precycled for three cycles at 0.4 A g^{-1}, and then subsequent cycle performance was at the specific current density. Electrochemical impedance spectroscopy (EIS) of the cells with different cycles was recorded by a Solartron electrochemical workstation between 0.01 and 10^5 Hz with an amplitude of 5 mV. Cyclic voltammetry (CV) was performed on the CHI660E electrochemical workstation between 0.01 and 1.2 V at a scan rate of 0.1 mV s^{-1}.

ASSOCIATED CONTENT

Supporting Information

The Supporting Information is available free of charge at https://pubs.acs.org/doi/10.1021/acsami.4c00590.

Materials and sample characterization, SEM of silicon particle, XRD results, FTIR spectra, ^{1}H NMR spectra, contact angle test, CV curves, SEM image, digital photographs, strain−stress curves, and cycling performance of the half cells (PDF)

AUTHOR INFORMATION

Corresponding Authors

Peng Zhang − *College of Energy, Xiamen University, Xiamen, Fujian 361102, China*; Phone: +86-05922186935; Email: pengzhang@xmu.edu.cn; Fax: +86-05922186935

Jinbao Zhao − *College of Energy, Xiamen University, Xiamen, Fujian 361102, China; State Key Laboratory of Physical Chemistry of Solid Surfaces, Collaborative Innovation Center of Chemistry for Energy Materials, Engineering Research Center of Electrochemical Technology, Ministry of Education, State-Province Joint Engineering Laboratory of Power Source Technology for New Energy Vehicle, College of Chemistry and Chemical Engineering, Xiamen University, Xiamen, Fujian 361005, China*; orcid.org/0000-0002-2753-7508; Phone: +86-05922186935; Email: jbzhao@xmu.edu.cn; Fax: +86-05922186935

Authors

Ruilai Ye − *College of Energy, Xiamen University, Xiamen, Fujian 361102, China*

Jiaxiang Liu − *College of Energy, Xiamen University, Xiamen, Fujian 361102, China*

Jianling Tian − *College of Energy, Xiamen University, Xiamen, Fujian 361102, China*

Yi Deng − *College of Energy, Xiamen University, Xiamen, Fujian 361102, China*

Xueying Yang − *College of Energy, Xiamen University, Xiamen, Fujian 361102, China*

Qichen Chen − *College of Energy, Xiamen University, Xiamen, Fujian 361102, China*

Complete contact information is available at: https://pubs.acs.org/10.1021/acsami.4c00590

Notes

The authors declare no competing financial interest.

ACKNOWLEDGMENTS

The authors gratefully acknowledge financial support from the National Key Research and Development Program of China (grant no. 2021YFB2400300), the National Natural Science Foundation of China (grant no. 21875195), the Key Project of Science and Technology of Xiamen (grant no. 3502Z20201013), and the Fundamental Research Funds for the Central Universities (grant no. 20720190040). The authors also would like to express gratitude for the support of Tan Kah Kee Innovation Laboratory.

REFERENCES

(1) Lu, J.; Chen, Z.; Pan, F.; Cui, Y.; Amine, K. High-Performance Anode Materials for Rechargeable Lithium-Ion Batteries. *Electrochem. Energy Rev.* **2018**, *1* (1), 35−53.

(2) Dong, Z.; Du, W.; Yan, C.; Zhang, C.; Chen, G.; Chen, J.; Sun, W.; Jiang, Y.; Liu, Y.; Gao, M.; et al. A Novel Tin-Bonded Silicon Anode for Lithium-Ion Batteries. *ACS Appl. Mater. Interfaces* **2021**, *13* (38), 45578−45588.

(3) Sanders, K. J.; Ciezki, A. A.; Berno, A.; Halalay, I. C.; Goward, G. R. Quantitative Operando 7Li NMR Investigations of Silicon Anode Evolution during Fast Charging and Extended Cycling. *J. Am. Chem. Soc.* **2023**, *145* (39), 21502−21513.

(4) Liu, T.; Chu, Q.; Yan, C.; Zhang, S.; Lin, Z.; Lu, J. Interweaving 3D Network Binder for High-Areal-Capacity Si Anode through Combined Hard and Soft Polymers. *Adv. Energy Mater.* **2018**, *9* (3), No. 1802645, DOI: 10.1002/aenm.201802645.

(5) Peng, X.; Liu, B.; Chen, J.; Jian, Q.; Li, Y.; Zhao, T. A Steric-Hindrance-Induced Weakly Solvating Electrolyte Boosting the Cycling Performance of a Micrometer-Sized Silicon Anode. *ACS Energy Lett.* **2023**, *8* (8), 3586−3594.

(6) Wang, F.; Li, P.; Li, W.; Wang, D. Electrochemical Synthesis of Multidimensional Nanostructured Silicon as a Negative Electrode Material for Lithium-Ion Battery. *ACS Nano* **2022**, *16* (5), 7689−7700.

(7) Nava, G.; Schwan, J.; Boebinger, M. G.; Mcdowell, M. T.; Mangolini, L. Silicon-Core−Carbon-Shell Nanoparticles for Lithium-Ion Batteries: Rational Comparison between Amorphous and Graphitic Carbon Coatings. *Nano Lett.* **2019**, *19* (10), 7236−7245.

(8) Harpak, N.; Davidi, G.; Patolsky, F. Breathing Parylene-Based Nanothin Artificial SEI for Highly-Stable Long Life Three-Dimensional Silicon Lithium-Ion Batteries. *Chem. Eng. J.* **2022**, *429*, No. 132077, DOI: 10.1016/j.cej.2021.132077.

(9) Wan, X.; Kang, C.; Mu, T.; Zhu, J.; Zuo, P.; Du, C.; Yin, G. A Multilevel Buffered Binder Network for High-Performance Silicon Anodes. *ACS Energy Lett.* **2022**, *7* (10), 3572−3580.

(10) Kim, J.; Kim, M.-S.; Lee, Y.; Kim, S.-Y.; Sung, Y.-E.; Ko, S. H. Hierarchically Structured Conductive Polymer Binders with Silver Nanowires for High-Performance Silicon Anodes in Lithium-Ion Batteries. *ACS Appl. Mater. Interfaces* **2022**, *14* (15), 17340−17347.

(11) Chang, H.; Wu, Y.-R.; Han, X.; Yi, T.-F. Recent Developments in Advanced Anode Materials for Lithium-Ion Batteries. *Energy Mater.* **2022**, *1* (1), No. 100003, DOI: 10.20517/energymater.2021.02.

(12) Li, G.; Guo, S.; Xiang, B.; Mei, S.; Zheng, Y.; Zhang, X.; Gao, B.; Chu, P. K.; Huo, K. Recent Advances and Perspectives of Microsized Alloying-Type Porous Anode Materials in High-Performance Li and Na-Ion Batteries. *Energy Mater.* **2022**, *2* (3), No. 200020, DOI: 10.20517/energymater.2022.24.

(13) Jiang, M.; Mu, P.; Zhang, H.; Dong, T.; Tang, B.; Qiu, H.; Chen, Z.; Cui, G. An Endotenon Sheath-Inspired Double-Network Binder Enables Superior Cycling Performance of Silicon Electrodes. *Nanomicro Lett.* **2022**, *14* (1), 87 DOI: 10.1007/s40820-022-00833-5.

(14) Kwon, T.-w.; Choi, J. W.; Coskun, A. The Emerging Era of Supramolecular Polymeric Binders in Silicon Anodes. *Chem. Soc. Rev.* **2018**, *47* (6), 2145−2164.

(15) Huang, W.; Wang, W.; Wang, Y.; Qu, Q.; Jin, C.; Zheng, H. Overcoming the Fundamental Challenge of PVDF Binder Use with Silicon Anodes with a Super-Molecular Nano-Layer. *J. Mater. Chem. A* **2021**, *9* (3), 1541−1551.

(16) Shin, D.; Park, H.; Paik, U. Cross-Linked Poly(acrylic acid)-Carboxymethyl Cellulose and Styrene-Butadiene Rubber as an Efficient Binder System and Its Physicochemical Effects on a High Energy Density Graphite Anode for Li-Ion Batteries. *Electrochem. Commun.* **2017**, *77*, 103−106.

(17) Liu, H.; Wu, Q.; Guan, X.; Liu, M.; Wang, F.; Li, R.; Xu, J. Ionically Conductive Self-Healing Polymer Binders with Poly(ether-thioureas) Segments for High-Performance Silicon Anodes in Lithium-Ion Batteries. *ACS Appl. Energy Mater.* **2022**, *5* (4), 4934−4944.

(18) Jung, C.-H.; Kim, K.-H.; Hong, S.-H. Stable Silicon Anode for Lithium-Ion Batteries through Covalent Bond Formation with a Binder via Esterification. *ACS Appl. Mater. Interfaces* **2019**, *11* (30), 26753−26763.

(19) Jiang, S.; Hu, B.; Shi, Z.; Chen, W.; Zhang, Z.; Zhang, L. Re-Engineering Poly(acrylic acid) Binder toward Optimized Electrochemical Performance for Silicon Lithium-Ion Batteries: Branching Architecture Leads to Balanced Properties of Polymeric Binders. *Adv. Funct. Mater.* **2019**, *30* (10), No. 1908558, DOI: 10.1002/adfm.201908558.

(20) Long, J.; He, W.; Liao, H.; Ye, W.; Dou, H.; Zhang, X. In Situ Prepared Three-Dimensional Covalent and Hydrogen Bond Synergistic Binder to Boost the Performance of SiOx Anodes for Lithium-Ion Batteries. *ACS Appl. Mater. Interfaces* **2023**, *15* (8), 10726−10734.

(21) Zhao, Y. M.; Yue, F. S.; Li, S. C.; Zhang, Y.; Tian, Z. R.; Xu, Q.; Xin, S.; Guo, Y. G. Advances of Polymer Binders for Silicon-Based Anodes in High Energy Density Lithium-Ion Batteries. *InfoMat* **2021**, *3* (5), 460−501.

(22) Lee, H. A.; Shin, M.; Kim, J.; Choi, J. W.; Lee, H. Designing Adaptive Binders for Microenvironment Settings of Silicon Anode Particles. *Adv. Mater.* **2021**, *33* (13), No. e2007460, DOI: 10.1002/adma.202007460.

(23) Song, J.; Zhou, M.; Yi, R.; Xu, T.; Gordin, M. L.; Tang, D.; Yu, Z.; Regula, M.; Wang, D. Interpenetrated Gel Polymer Binder for High-Performance Silicon Anodes in Lithium-Ion Batteries. *Adv. Funct. Mater.* **2014**, *24* (37), 5904−5910.

(24) Chen, H.; Wu, Z.; Su, Z.; Chen, S.; Yan, C.; Al-mamun, M.; Tang, Y.; Zhang, S. A Mechanically Robust Self-Healing Binder for Silicon Anode in Lithium Ion Batteries. *Nano Energy* **2021**, *81*, No. 105654.

(25) Roy, A.; Manna, K.; Dey, S.; Pal, S. Chemical Modification of β-cyclodextrin towards Hydrogel Formation. *Carbohydr. Polym.* **2023**, *306*, No. 120576, DOI: 10.1016/j.carbpol.2023.120576.

(26) Shi, Z.; Liu, Q.; Yang, Z.; Robertson, L. A.; Bheemireddy, S. R.; Zhao, Y.; Zhang, Z.; Zhang, L. A Chemical Switch Enabled Autonomous Two-Stage Crosslinking Polymeric Binder for High Performance Silicon Anodes. *J. Mater. Chem. A* **2022**, *10* (3), 1380−1389.

(27) Huang, Z.; Wang, L.; Xu, Y.; Fang, L.; Li, H.; Zhu, B.; Song, Y. Bifunctional Binder Enables Controllable Deposition of Polysulfides for High-Loading Li-S Battery. *Chem. Eng. J.* **2022**, *443*, No. 136347, DOI: 10.1016/j.cej.2022.136347.

(28) Shi, Z.; Jiang, S.; Robertson, L. A.; Zhao, Y.; Sarnello, E.; Li, T.; Chen, W.; Zhang, Z.; Zhang, L. Restorable Neutralization of Poly(acrylic acid) Binders toward Balanced Processing Properties and Cycling Performance for Silicon Anodes in Lithium-Ion Batteries. *ACS Appl. Mater. Interfaces* **2020**, *12* (52), 57932−57940.

(29) Wan, X.; Mu, T.; Shen, B.; Meng, Q.; Lu, G.; Lou, S.; Zuo, P.; Ma, Y.; Du, C.; Yin, G. Stable Silicon Anodes Realized by Multifunctional Dynamic Cross-Linking Structure with Self-Healing Chemistry and Enhanced Ionic Conductivity for Lithium-Ion Batteries. *Nano Energy* **2022**, *99*, No. 107334, DOI: 10.1016/j.nanoen.2022.107334.

(30) Wang, Y.; Xu, H.; Chen, X.; Jin, H.; Wang, J. Novel Constructive Self-Healing Binder for Silicon Anodes with High Mass Loading in Lithium-Ion Batteries. *Energy Storage Mater.* **2021**, *38*, 121−129.

(31) Sun, R.; Hu, J.; Shi, X.; Wang, J.; Zheng, X.; Zhang, Y.; Han, B.; Xia, K.; Gao, Q.; Zhou, C.; et al. Water-Soluble Cross-Linking Functional Binder for Low-Cost and High-Performance Lithium−Sulfur Batteries. *Adv. Funct. Mater.* **2021**, *31* (42), No. 2104858, DOI: 10.1002/adfm.202104858.

(32) Jiang, H.-W; Yang, Y.; Nie, Y.-M.; Su, Z.-F.; Long, Y.-F.; Wen, Y.-X; Su, J. Cross-Linked β-CD-CMC as an Effective Aqueous Binder for Silicon-Based Anodes in Rechargeable Lithium-Ion Batteries. *RSC Adv.* **2022**, *12* (10), 5997−6006.

(33) Chen, M.; Zou, C.; Tang, W.; Cao, Y. Stable Hydrogen Bonding Interactions in Supramolecular Deep Eutectic Solvents Based on Carbon Quantum Dots: For Extraction and Oxidative Desulfuriza-

tion. *Sep. Purif. Technol.* **2023**, *323*, No. 124491, DOI: 10.1016/j.seppur.2023.124491.
(34) Lin, X.; Wen, Y.; Wang, J.; Shang, H.; Liu, H.; Xu, X. Boston Ivy-Inspired Natural-Rich Binder with Strong Adhesion for Advanced Silicon-Based Anodes. *Chem. Eng. J.* **2023**, *468*, No. 143784, DOI: 10.1016/j.cej.2023.143784.
(35) Jiang, Y.; Mu, D.; Chen, S.; Wu, B.; Cheng, K.; Li, L.; Wu, F. Electrochemical Performance of Si Anode Modified with Carbonized Gelatin Binder. *J. Power Sources* **2016**, *325*, 630−636.
(36) Jing, Z.; Zhang, Q.; Liang, Y. Q.; Zhang, Z.; Hong, P.; Li, Y. Synthesis of Poly(acrylic acid)−Fe3+/Gelatin/Poly(vinyl alcohol) Triple-Network Supramolecular Hydrogels with High Toughness, High Strength and Self-Healing Properties. *Polym. Int.* **2019**, *68* (10), 1710−1721.
(37) Ye, C.; Tu, W.; Yin, L.; Zheng, Q.; Wang, C.; Zhong, Y.; Zhang, Y.; Huang, Q.; Xu, K.; Li, W. Converting Detrimental HF in Electrolytes into a Highly Fluorinated Interphase on Cathodes. *J. Mater. Chem. A* **2018**, *6* (36), 17642−17652.
(38) Tang, W.-J.; Peng, W.-J.; Yan, G.-C.; Guo, H.-J.; Li, X.-H.; Zhou, Y. Effect of Fluoroethylene Carbonate as an Electrolyte Additive on the Cycle Performance of Silicon-Carbon Composite Anode in Lithium-Ion Battery. *Ionics* **2017**, *23* (12), 3281−3288.
(39) Kim, W.-J.; Kang, J. G.; Kim, D.-W. Blood Clot-Inspired Viscoelastic Fibrin Gel: New Aqueous Binder for Silicon Anodes in Lithium Ion Batteries. *Energy Storage Mater.* **2022**, *45*, 730−740.
(40) Zhang, B.; Dong, Y.; Han, J.; Zhen, Y.; Hu, C.; Liu, D. Physicochemical Dual Cross-Linking Conductive Polymeric Networks Combining High Strength and High Toughness Enable Stable Operation of Silicon Microparticle Anodes. *Adv. Mater.* **2023**, *35* (29), No. e2301320, DOI: 10.1002/adma.202301320.
(41) Zhao, J.; Wei, D.; Wang, J.; Yang, K.; Wang, Z.; Chen, Z.; Zhang, S.; Zhang, C.; Yang, X. Inorganic Crosslinked Supramolecular Binder with Fast Self-Healing for High Performance Silicon Based Anodes in Lithium-Ion Batteries. *J. Colloid Interface Sci.* **2022**, *625*, 373−382.
(42) Reddy, B. R. S.; Ahn, J.-H.; Ahn, H.-J.; Cho, G.-B.; Cho, K.-K. Low-Cost and Sustainable Cross-Linked Polyvinyl Alcohol−Tartaric Acid Composite Binder for High-Performance Lithium−Sulfur Batteries. *ACS Appl. Energy Mater.* **2023**, *6* (11), 6327−6337.

https://doi.org/10.1021/acsami.4c00590
ACS Appl. Mater. Interfaces 2024, 16, 16820−16829